bioRxiv preprint doi: https://doi.org/10.1101/169698; this version posted July 28, 2017. The copyright holder for this preprint (which was not certified by peer review) is the author/funder, who has granted bioRxiv a license to display the preprint in perpetuity. It is made available under aCC-BY 4.0 International license.

Neuronal origin of the temporal dynamics of spontaneous BOLD activity correlation

Teppei Matsui[1,2*], Tomonari Murakami[1,2] and Kenichi Ohki[1,2*]

1. Department of Physiology, The University of Tokyo School of Medicine, Tokyo 113-0033, Japan
2. Department of Molecular Physiology, Graduate School of Medical Sciences, Kyushu University, Fukuoka, Japan

Send Correspondence To:

Teppei Matsui, Ph.D. (Email: tematsui@m.u-tokyo.ac.jp)

or

Kenichi Ohki, M.D, Ph.D. (Email: kohki@m.u-tokyo.ac.jp)

Department of Physiology

The University of Tokyo School of Medicine

Tokyo 113-0033, Japan

Phone: (+81)-3-5841-3459

bioRxiv preprint doi: https://doi.org/10.1101/169698; this version posted July 28, 2017. The copyright holder for this preprint (which was not certified by peer review) is the author/funder, who has granted bioRxiv a license to display the preprint in perpetuity. It is made available under aCC-BY 4.0 International license.

Abstract (196/200 words)

Resting-state functional connectivity (FC) has become a major fMRI method to study network organization of human brains. There is recent interest in the temporal fluctuations of FC calculated using short time-windows ("dynamic FC") because it could provide information inaccessible with conventional "static" FC that is typically calculated using the entire scan lasting several tens of minutes. Although multiple studies have revealed considerable temporal fluctuations in FC, it is still unclear whether the fluctuations of FC measured in hemodynamics reflect the dynamics of underlying neural activity. We addressed this question using simultaneous imaging of neuronal calcium and hemodynamic signals in mice, and found coordinated temporal dynamics of calcium FC and hemodynamic FC measured in the same short time windows. Moreover, we found that variation in transient neuronal coactivation patterns (CAPs) was significantly related to temporal fluctuations of sliding window FC in hemodynamics. Finally, we show that observed dynamics of FC cannot be fully accounted for by simulated data assuming stationary FC. These results provide evidence for the neuronal origin of dynamic FC and further suggest that information relevant to FC is condensed in temporally sparse events that can be extracted using a small number of time points.

Keywords: calcium imaging, BOLD, resting state, functional connectivity, stationarity

bioRxiv preprint doi: https://doi.org/10.1101/169698; this version posted July 28, 2017. The copyright holder for this preprint (which was not certified by peer review) is the author/funder, who has granted bioRxiv a license to display the preprint in perpetuity. It is made available under aCC-BY 4.0 International license.

Introduction

Resting state functional connectivity (FC) uses temporal correlation of spontaneous neuronal activity to assess network organization of brain regions in a non-invasive manner (Fox and Raichle 2007). Traditionally, FC has been calculated using all time points in a scan that typically lasts between several minutes to tens of minutes (Biswal et al. 1995; Fox et al. 2005; Van Dijk et al. 2010). Such "static" FC has been shown to largely reflect anatomical connectivity (Adachi et al. 2012; Honey et al. 2009; Matsui et al. 2012; Matsui et al. 2011; Vincent et al. 2007). Recently, in contrast to traditional analysis of "static" FC, the temporal fluctuation of FC across short time windows is increasingly recognized as a useful aspect of FC (Allen et al. 2014; Hutchison et al. 2013; Zalesky et al. 2014). Such "dynamic" FC calculated using short time-windows could provide information that is inaccessible with static FC about the functional network organizations of healthy and diseased brains (Calhoun et al. 2014; Preti et al. 2016). The presence of temporal fluctuations in FC has also informed theoreticians to constrain realistic models of brain networks (Deco et al. 2013; Hansen et al. 2015; Messé et al. 2014).

However, despite growing interest, the neurophysiological basis of dynamic FC is still weak. Previous attempts to investigate neural origin of dynamic FC by simultaneous measurement of electrophysiological and functional magnetic resonance imaging (fMRI) are limited in several ways (Lu et al. 2007; Pan et al. 2011; Tagliazucchi et al. 2012b; Thompson et al. 2013). In some studies, electrophysiological recording was limited to a small number of recording sites due to technical difficulty (Lu et al. 2007; Pan et al. 2011; Thompson et al. 2013); hence, information on the global pattern of neuronal activity was lacking. In another study, electrophysiological signals were obtained with an electroencephalogram, which records global neuronal activity but lacks precise spatial information (Tagliazucchi et al. 2012b). Thus, the link between temporal fluctuations of FC in hemodynamics and that of large-scale neuronal activity has not been adequately proven.

Several studies have also questioned whether the apparent "dynamics" of FC calculated using the sliding window method is related to temporal instability of spontaneous brain network (Hindriks et al. 2016; Laumann et al. 2016). While many studies have attributed temporal fluctuations of sliding window FC to non-stationarity of spontaneous neuronal activity correlation (Allen et al. 2014; Zalesky et al. 2014),

bioRxiv preprint doi: https://doi.org/10.1101/169698; this version posted July 28, 2017. The copyright holder for this preprint (which was not certified by peer review) is the author/funder, who has granted bioRxiv a license to display the preprint in perpetuity. It is made available under aCC-BY 4.0 International license.

some recent studies have demonstrated that the temporal fluctuations of FC observed in the real and the simulated data, which is stationary by construction, are statistically indistinguishable (Hindriks et al. 2016; Laumann et al. 2016). Furthermore, Laumann and colleagues have shown that, in the human resting-state fMRI data, a large portion of non-stationarity in FC is attributed to head motion, and eliminating data with excessive head motion substantially decreases the non-stationarity of FC (Laumann et al. 2016). Therefore, not only the neuronal basis of dynamic FC, but also the existence of statistical non-stationarity of FC, or at least the capability of sliding window methods to detect the non-stationarity, is called into question.

In the present study, we addressed these questions using simultaneous imaging of neuronal calcium and blood oxygen level dependent (BOLD) hemodynamic signals in the entire neocortex of transgenic mice expressing a genetically encoded calcium indicator (Matsui et al. 2016; Vanni and Murphy 2014; White et al. 2011). In the present experimental setup, wide-field calcium signal provided access to neuronal activity at higher temporal resolution and signal-to-noise ratio compared to that of hemodynamic signal (Matsui et al. 2016; Murakami et al. 2015; Tohmi et al. 2014; Vanni and Murphy 2014). Moreover, unlike human fMRI data, in the present dataset, mice were tightly head-fixed and lightly anesthetized; thus, excluding head motions from contaminating FC. Main findings of the present study are as follows. First, we found consistency between the dynamics of FC calculated using calcium and hemodynamic signals, suggesting the neuronal origin of the temporal fluctuations of hemodynamic FC. Second, we found that temporal fluctuations of the spatial pattern of transient neuronal coactivations as measured in calcium signal were significantly correlated with temporal fluctuations of hemodynamic FC. Finally, we found that statistical properties of sliding window FC were significantly different between the real and the simulated data suggesting non-stationarity of resting-state FC.

bioRxiv preprint doi: https://doi.org/10.1101/169698; this version posted July 28, 2017. The copyright holder for this preprint (which was not certified by peer review) is the author/funder, who has granted bioRxiv a license to display the preprint in perpetuity. It is made available under aCC-BY 4.0 International license.

Materials and Methods

Animals

Emx1-IRES-cre and Ai38 (Zariwala et al. 2012) mice were obtained from the Jackson Laboratory (Sacramento, CA). These mice were crossed and all cortical excitatory neurons expressed GCaMP3. Mice (P60–P90) were prepared for *in vivo* wide-field simultaneous imaging. Anesthesia was induced with isoflurane (3 %) and maintained with isoflurane (1 – 2 % in surgery, 0.5 – 0.8 % during imaging) and chlorprothixene (0.3 – 0.8 mg/kg, intramuscular injection). For simultaneous imaging of calcium and hemodynamic signals, a custom-made metal head plate was attached to the skull using dental cement (Sun Medical Company, Ltd, Shiga, Japan) and a large craniotomy was made over the whole cortex. The craniotomy was sealed with 1 % agarose and a glass coverslip. During the imaging, body temperature was maintained by a heat pad. All experiments were carried out in accordance with the NIH Guide for the Care and Use of Laboratory Animals, the institutional animal welfare guidelines set forth by the Animal Care and Use Committee of Kyushu University, and the study was approved by the Ethical Committee of Kyushu University.

Simultaneous Calcium and Intrinsic Signal Imaging

The data for simultaneous imaging of calcium and hemodynamic signals was taken from a published report (Matsui et al. 2016). Briefly, simultaneous imaging of calcium and intrinsic signals *in vivo* was performed using a macro zoom fluorescence microscope (MVX-10, Olympus, Tokyo, Japan) or an upright fluorescence microscope (ECLIPSE Ni-U, Nikon, Tokyo, Japan), equipped with a 1x objective. A 625 nm LED light source was used to obtain intrinsic signals. GCaMP was excited by a 100 W mercury lamp through a GFP mirror unit (Olympus). Intrinsic signal data was collected at a frame rate of 5 Hz using a CCD camera (1,000m; Adimec, Boston, MA, U.S.A.) and calcium signal data was collected at a frame rate of 10 Hz using a CCD camera (DS-Qi1 Mc; Nikon). The emission filters were 625 nm long pass (SC-60, Fuji film, Tokyo, Japan) for intrinsic signals, and 505-535 nm band pass (FF01-520/35-25, Semrock, Lake Forest, Illinois) for calcium signals. Data were acquired for 30-60 min per animal (5 min per scan).

Data Preprocessing

bioRxiv preprint doi: https://doi.org/10.1101/169698; this version posted July 28, 2017. The copyright holder for this preprint (which was not certified by peer review) is the author/funder, who has granted bioRxiv a license to display the preprint in perpetuity. It is made available under aCC-BY 4.0 International license.

All data analyses were conducted in Matlab (MathWorks, Natick, MA) using a method described previously (Matsui et al. 2016). Briefly, all the image frames were corrected for possible within-scan motion by rigid-body transformation. Calcium and hemodynamic images were then coregistered by rigid-body transformation using manually selected anatomical landmarks that were visible in both images (e.g., branching points of blood vessels). All of the images were then spatially down-sampled by a factor of two. Pixels within the cortex (at this point including large blood vessels including the sinus) were extracted manually. For both calcium and hemodynamics, slow drift in each pixel's time course was removed using a high-pass filter (> 0.01 Hz, second order Butterworth. No low-pass filter was used). After filtering, each pixel's time course was normalized by subtracting the mean across time and then dividing by the standard deviation across time. Global signal regression was conducted by regressing out the time course of average signal within the brain from each pixel's time course. Finally, hemodynamic signal was multiplied by -1 to set the polarity of the activity change equal to that in the calcium signal.

Extraction of Region-of-Interest (ROI) Time Courses

Selection of ROI and time courses are conducted as described previously (Matsui et al. 2016). Briefly, 38 cortical regions (19 for each hemisphere) were selected as ROIs based on a previous mouse functional connectivity study (White et al. 2011) (Supplementary Fig. 1). Each ROI was a 6 × 6 pixel square (0.5 mm × 0.5 mm) centered at a selected coordinate. The time course for each ROI was calculated by averaging the time courses of pixels within the ROI that corresponded to gray matter. ROIs located outside of the FOV were discarded.

Analysis of FC

For both calcium and hemodynamic signals, FC was calculated using a standard seed-based correlation method (Matsui et al. 2016). First, the correlation coefficient between the time course of a selected ROI ("seed time course") and the time course of every pixel within the brain was calculated. Second, FC values were averaged across scans to obtain FC values for each pixel. The spatial correlation between FC maps of calcium and hemodynamic signals was calculated by taking the pixel-by-pixel correlation coefficient between the two maps using all the gray matter pixels. FC with

bioRxiv preprint doi: https://doi.org/10.1101/169698; this version posted July 28, 2017. The copyright holder for this preprint (which was not certified by peer review) is the author/funder, who has granted bioRxiv a license to display the preprint in perpetuity. It is made available under aCC-BY 4.0 International license.

short time window was obtained by taking correlation coefficient using all the frames within a 30-sec window. Steps of 3 sec and 30 sec were used for the sliding window and non-overlapping window, respectively. Scan-shifted control was calculated by shifting the scan number of hemodynamics data relative to simultaneously obtained calcium data.

Analysis of CAPs

CAP analysis was adopted from previous fMRI studies (Liu and Duyn 2013). Briefly, calcium time course from each ROI was z-normalized. Then, frames corresponding to peaks of the time course whose height exceeded 2 s.d. were considered CAPs of the ROI. For a given ROI, comparison between FC map within a sliding window and CAPs contained in the window was conducted by calculating spatial correlation between the FC map and the summed spatial pattern of CAPs contained within the window (i.e. adding all the frames corresponding to CAPs within the window). Comparison between CAPs and short window FC using all ROIs were performed as follows. First, for a given scan, for all the ROIs, CAPs were calculated for calcium signal. For each ROI, multiple CAPs were averaged to yield mean CAP for the scan (CAP_{scan}). For hemodynamic signal, FC map was calculated for each ROI (FC_{scan}). For a given pairs of ROIs (i and j), correlation between the pair of corresponding CAP_{scan} was calculated [$R(CAP_{scan})_{ij}$]. Corresponding correlation between the pair of FC maps was also calculated for each pair of ROIs [$R(FC_{scan})_{ij}$]. Second, for a given 30-sec window in the scan, for all the ROIs, CAPs were detected for calcium signal. For each ROI, multiple CAPs were averaged to yield mean CAP within the window (CAP_{window}). FC map was also calculated using hemodynamic signal within the window (FC_{window}). Then, for a given pairs of ROIs (i and j), correlation between the pair of corresponding CAP_{window} was calculated [$R(CAP_{window})_{ij}$]. Then difference between the $R(CAP_{window})_{ij}$ and $R(CAP_{scan})_{ij}$ was taken as the index of deviation from the mean pattern for the given window [$\Delta CAP_{ij} = R(CAP_{window})_{ij} - R(CAP_{scan})_{ij}$]. Similarly, ΔFC_{ij} was obtained by subtracting $R(FC_{scan})_{ij}$ from $R(FC_{window})_{ij}$. Finally, correlation coefficient between non-diagonal elements of the matrices of ΔCAP and ΔFC were calculated. When CAPs were absent for a particular ROI in a time window, that ROI was omitted from the calculation for the time window.

bioRxiv preprint doi: https://doi.org/10.1101/169698; this version posted July 28, 2017. The copyright holder for this preprint (which was not certified by peer review) is the author/funder, who has granted bioRxiv a license to display the preprint in perpetuity. It is made available under aCC-BY 4.0 International license.

201 ***Cluster Analysis and Kurtosis Analysis***

202 For the state analysis of sliding window FC, we adopted the k-means clustering
203 algorithm used in the previous studies (Allen et al. 2014; Laumann et al. 2016).
204 Correlation distance (1-r) was used to compute the separation between each window's
205 FC-matrix (using all 38 ROIs) and the k-means clustering was iterated 100 times with
206 random centroid positions to avoid local minima. The windowed FC-matrices were
207 mean-centered by scan to eliminate scan-level and subject-level features from
208 contributing the clustering result. K-means clustering was applied in the same manner to
209 the simulated data that was matched in size to the real data. The cluster validity index
210 was used to evaluate the quality of clustering for the range of cluster numbers (k = 2-10).
211 The cluster validity index was computed as the average ratio of within-cluster distance
212 to between-cluster distance.

213 Non-stationarity of spontaneous neuronal signal correlation was assessed by
214 calculating multivariate kurtosis using the same procedure as described by Laumann
215 and colleagues (Laumann et al. 2016). One value of kurtosis was calculated for each
216 FC-matrix (using all 38 ROIs) obtained each scan. The same procedure was applied to
217 the simulated data that was matched in size to the real data.

218

219 ***Time Course Simulation***

220 To obtain a null dataset to evaluate the non-stationarity of the real data, we constructed
221 simulated time courses using a method developed by Laumann and colleagues
222 (Laumann et al. 2016). Briefly, random normal deviates having the same dimensionality
223 as a real dataset are sampled. These time courses are multiplied in the spectral domain
224 by the average power spectrum of the (bandpass filtered) real data. These time courses
225 are then projected onto the eigenvectors derived from the covariance matrix of the real
226 data. This procedure produces simulated data that are stationary by construction but
227 matched to real data in the covariance structure and mean spectral content.

228

bioRxiv preprint doi: https://doi.org/10.1101/169698; this version posted July 28, 2017. The copyright holder for this preprint (which was not certified by peer review) is the author/funder, who has granted bioRxiv a license to display the preprint in perpetuity. It is made available under aCC-BY 4.0 International license.

Results

Consistent FC dynamics in calcium and hemodynamic signals

Transgenic mice expressing GCaMP in neocortical neurons were used to simultaneously measure neuronal calcium signal and hemodynamics in a large portion of bilateral neocortex (Fig. 1A) (Matsui et al. 2016). Mice were lightly anesthetized and head-fixed with metal plates so that head-motion could not contaminate the signals. We used sliding window correlation (30 sec window at 3 sec steps) to examine if FC in mice exhibited dynamic changes. Consistent with previous reports in humans (Allen et al. 2014; Chang and Glover 2010; Zalesky et al. 2014) and other animals (Hutchison et al. 2014; Majeed et al. 2009), FC between pairs of ROIs calculated with sliding windows showed considerable variability over different time points both in calcium signal and hemodynamics (Fig. 1B-C). Consistent with the notion that variability in hemodynamic FC arises from underlying neuronal activity, we found close matches between dynamics of FC in calcium and hemodynamics (correlation coefficients, 0.631 and 0.675 for Figs. 1B and 1C, respectively). Correlation between the time courses of calcium FC and hemodynamic FC was significantly larger for the data than that of the scan-shifted control ($P < 10^{-20}$, Kolmogorov-Smirnov test; Fig. 1D).

To further examine the consistency between the dynamics of FC in calcium and hemodynamics in the entire neocortex, we calculated FC among all pairs of ROIs and compared them across time windows (Fig. 2A-B). The ROI-based FC-matrices in calcium and hemodynamics both showed variability across time windows. On the other hand, FC matrices in calcium and hemodynamics within each time window were similar. If the dynamics of FC in calcium and hemodynamics were matched, the similarity between calcium and hemodynamic FC in the same time window should be higher than that calculated using different time windows (e.g., similarity between $Ca\text{-}FC_{window\#1}$ and $Hemo\text{-}FC_{window\#1}$ would be higher than the similarity between $Ca\text{-}FC_{window\#1}$ and $Hemo\text{-}FC_{window\#2}$). Otherwise, the similarity between FC-matrices in calcium and hemodynamics merely reflects the overall similarity of FC in calcium and hemodynamics but not the coordinated dynamics of calcium and hemodynamic FC. Across all the data, we found that the distribution of the correlation coefficient between the FC-matrices in calcium and hemodynamics was shifted toward positive values compared with that calculated with the scan-shifted data ($P < 10^{-14}$, Kolmogorov-Smirnov test; Fig. 2C). The difference between the real data and the

bioRxiv preprint doi: https://doi.org/10.1101/169698; this version posted July 28, 2017. The copyright holder for this preprint (which was not certified by peer review) is the author/funder, who has granted bioRxiv a license to display the preprint in perpetuity. It is made available under aCC-BY 4.0 International license.

trial-shifted data was also consistently positive across animals ($p < 0.0156$, $n = 7$ mice, sign-rank test; Fig. 2D) and was seen across various window sizes ranging from 1 sec to 60 sec (Fig. 2E). Together these results suggest that temporal variability in hemodynamic FC, as measured with sliding window, arises from neural activity rather than from movement-related artifacts (Laumann et al. 2016) or non-neuronal physiological artifacts such as heartbeat and respiration (Bianciardi et al. 2009; Shmueli et al. 2007).

Variations in transient neuronal coactivations explained variations in FC

What are the potential neuronal events that create dynamic FC? Recent fMRI studies proposed that variability in the neuronal coactivation pattern (CAP) of brain areas is directly reflected in the dynamic change of FC observed with the sliding window correlation (Liu and Duyn 2013). To address this possibility, we compared sliding window FC in hemodynamics with the CAPs calculated in the calcium signal. The use of calcium signal for extracting CAPs allowed us to capture faster spatiotemporal dynamics than the hemodynamics. More importantly, the use of two different signals also allowed us to avoid comparing sliding window FC and CAPs that were derived from the same signals and could lead to circular logic.

For each anatomical ROI, we first detected peaks in the calcium signal within a given time-window and then defined CAPs as the frames in the calcium signal corresponding to the detected peak locations (Fig. 3A) (Liu and Duyn 2013). Similar to the previous reports in fMRI (Liu et al. 2013; Liu and Duyn 2013), we found variations in the spatial patterns of CAPs extracted from the same ROI (Fig. 3A, panels above time courses). We next examined if the variations of the spatial pattern of CAPs could explain that of sliding window FC. For each ROI in each 30 sec window, we extracted CAPs and FC using calcium and hemodynamic signals, respectively. In the example 30 sec windows shown in Figure 3A, time courses of the chosen ROI showed transient activations that resulted in 11 and 3 frames of CAPs (corresponding to 1.1 and 0.3 sec of data, respectively). Despite the small number of frames corresponding to CAPs, the average spatial pattern of CAPs in the time window closely matched the spatial pattern of hemodynamic FC calculated in the same time window (compare mean CAP and mean FC in Fig. 3A).

To further compare CAPs with sliding window hemodynamic FC across ROIs, we

bioRxiv preprint doi: https://doi.org/10.1101/169698; this version posted July 28, 2017. The copyright holder for this preprint (which was not certified by peer review) is the author/funder, who has granted bioRxiv a license to display the preprint in perpetuity. It is made available under aCC-BY 4.0 International license.

295 calculated CAPs for all pairs of ROIs and compared them with FC of the same
296 ROI-pairs in the same time window (Fig. 3B). Across all the data, CAP-matrices and
297 FC matrices showed high positive correlation (Fig. 3C-D; mean R = 0.525 across
298 animals) suggesting that CAP and FC calculated using the same sliding window were
299 similar.
300 The similarity between CAP and FC does not necessarily indicate coordinated
301 temporal variation between CAPs and FCs in individual time-window, but could result
302 entirely from similarity between the time-average patterns of CAP and FC. Therefore, to
303 further examine if coordinated temporal variations in CAPs and FCs exist, we
304 calculated ΔCAP and ΔFC by subtracting from each CAP and FC in each time window
305 the average pattern (i.e. average in the entire scan) of CAP and FC, respectively (Fig.
306 4A). We found that the distribution of the correlation between ΔCAP and ΔFC for the
307 real data was shifted toward positive values whereas the same distribution calculated
308 using trial-shifted data was centered near zero ($P < 10^{-30}$, Kolmogorov-Smirnov test; Fig.
309 4B). Furthermore, the correlation between ΔCAP and ΔFC was consistently positive
310 across all animals ($P < 0.156$, n = 7 mice, sign rank test; Fig. 4C) and was seen across
311 various sizes of time-windows ranging from 1 to 60 sec (Fig. 4D). Taken together, these
312 results suggest temporal fluctuations of the spatial pattern of CAPs at least partly
313 explain temporal fluctuations of hemodynamic FC.
314
315 ***Dynamics of FC arise from non-stationarity of resting-state activity***
316 Because FC is estimated by using finite number of time-points, temporal fluctuations of
317 FC observed in short time-windows could arise from mere sampling error even when
318 underlying FC is stationary (Laumann et al. 2016). We next addressed whether the
319 sampling error could explain the dynamics of FC observed in the present data. We
320 compared two indices used in a previous study, namely cluster validity index and
321 kurtosis, for real data and simulated data that are matched in spectral and covariance
322 properties (Fig. 5A) (Laumann et al. 2016). The cluster validity index measures degree
323 of clustering of multiple sliding window FC calculated within the scan. Note that
324 smaller cluster validity index indicates more clustering (see Methods for details). For
325 both calcium and hemodynamic signals, we found cluster validity index of real data to
326 be significantly smaller than that of simulated data (Fig. 5B), suggesting that the real
327 data had cluster structure that could not be fully accounted for by sampling error.

bioRxiv preprint doi: https://doi.org/10.1101/169698; this version posted July 28, 2017. The copyright holder for this preprint (which was not certified by peer review) is the author/funder, who has granted bioRxiv a license to display the preprint in perpetuity. It is made available under aCC-BY 4.0 International license.

328 Similarly, we calculated kurtosis of the covariance matrices of real and simulated data.
329 If the kurtosis of real data were larger than that of simulated data that is stationary by
330 construction, the non-stationarity of the real data is implied. We found that the kurtosis
331 of the real data was significantly higher than that of the simulated data ($P < 10^{-11}$ for
332 both, sign rank test, n = 64 scans; Fig. 5C). Together, these results suggest that
333 dynamics of FC arise from non-stationarity of spontaneous neuronal activity, and
334 analyses based on sliding window correlation have the potential to detect
335 non-stationarity.
336

bioRxiv preprint doi: https://doi.org/10.1101/169698; this version posted July 28, 2017. The copyright holder for this preprint (which was not certified by peer review) is the author/funder, who has granted bioRxiv a license to display the preprint in perpetuity. It is made available under aCC-BY 4.0 International license.

Discussion

In the present study, we used simultaneous imaging of calcium and hemodynamic signals to show that temporal fluctuations in hemodynamic FC calculated in a short time window closely follow that of calcium FC, suggesting the neuronal origin of dynamic FC. We have further shown that the spatial pattern of hemodynamic FC in a short time window is predicted by averaging transient coactivations in the calcium signal (CAPs) contained within the same time-window suggesting that temporally interspersed transient neuronal events underlie resting-state FC. Finally, we have shown that in both calcium and hemodynamic signals, statistical properties of FC calculated in a short time window was significantly different from that obtained with simulated signals that were stationary by construction. These results advocate for the analysis of the dynamic aspect of FC obtained in human fMRI experiments. Insights of the neuronal events underlying dynamic FC provided by the present study would also be informative for developing appropriate analysis methods for dynamic FC.

Relationship to previous investigations of the neuronal origin of dynamic FC

To provide direct evidence linking neuronal activity and dynamic FC, several groups have conducted simultaneous recording of fMRI and local field potential (LFP) (Lu et al. 2007; Pan et al. 2011; Thompson et al. 2013) or EEG (Chang et al. 2013; Tagliazucchi et al. 2012b). However, these previous studies were limited in several ways. Since LFP recordings were limited from a small number of recording sites whereas EEG recording did not have enough spatial resolution, evidence directly linking global spatial pattern of neuronal activity with hemodynamic FC has been lacking. Using simultaneous imaging of calcium and hemodynamic signals, the present study provides evidence suggesting that temporal variability of hemodynamic FC and its time-to-time spatial patterns reflect spatial patterns of large-scale neuronal activity. Moreover, since the present study used anesthetized and head-fixed mice, the results are unlikely to be attributable to head motion.

Recent human fMRI studies have proposed that neuronal activity important for FC is condensed into transient large scale neuronal coactivations (i.e. CAPs) (Liu and Duyn 2013; Tagliazucchi et al. 2012a; Tagliazucchi et al. 2011). Consistent with this idea, imaging studies in mice revealed transient neuronal coactivations across brain areas (Matsui et al. 2016; Mohajerani et al. 2013; Vanni and Murphy 2014). In our previous

bioRxiv preprint doi: https://doi.org/10.1101/169698; this version posted July 28, 2017. The copyright holder for this preprint (which was not certified by peer review) is the author/funder, who has granted bioRxiv a license to display the preprint in perpetuity. It is made available under aCC-BY 4.0 International license.

study, we searched for neuronal coactivations that resembled the spatial patterns of (static) FC and showed that such neuronal coactivations were converted into spatially similar hemodynamic signals (Matsui et al. 2016). In the present study, we took a different approach that was similar to single frame analysis methods employed in recent human fMRI studies (Karahanoğlu and Van De Ville 2015; Liu et al. 2013; Liu and Duyn 2013; Tagliazucchi et al. 2011). Instead of specifically looking at neuronal coactivations that resembled "static" FC, we took all the individual coactivations (CAPs) into our analysis and showed that variation of the spatial pattern of individual CAPs across time windows was significantly related to variations of hemodynamic FC across time windows. Thus, the present findings suggest importance of the development of analysis that specifically focuses on CAPs (Karahanoğlu and Van De Ville 2015; Liu et al. 2013). It should be noted that, although statistically significant, the correlation between ΔCAP and ΔFC was relatively weak. Part of the reason for this could be non-neuronal physiological noise that contributed to hemodynamics (Matsui et al. 2016). In the present study, because of the use of anesthesia and head-fixation, head motion is unlikely to be the primary source of the non-neuronal noise. However, other physiological activities, e.g. respiration and heartbeat, are known to affect hemodynamics (Chang et al. 2009; Chang and Glover 2009) and, thus, likely to affect temporal fluctuation of hemodynamic FC as well. Our results (i.e. relatively low correlation between ΔCAP and ΔFC) indicate that correction for such non-neuronal physiological noise (Glover et al. 2000) is likely to be essential for the analysis of dynamic FC.

Non-stationarity of spontaneous brain activity correlation

It has been of a matter of debate to what extent temporal fluctuations of FC is attributed to the dynamics of underlying neuronal activity but not to non-neuronal sources of noise (e.g., head motion, sampling variability; reviewed in (Hutchison et al. 2013)). Laumann and colleagues have reported that most of the temporal fluctuations of single subject FC is explained by head motion (Laumann et al. 2016). After controlling for the head motion, Laumann and colleagues have concluded that statistical properties of resting-state FC in human fMRI is indistinguishable from those obtained with simulated signals that are stationary by construction. A similar study by Hindriks and colleagues has also indicated the apparent dynamics of FC calculated with the sliding

bioRxiv preprint doi: https://doi.org/10.1101/169698; this version posted July 28, 2017. The copyright holder for this preprint (which was not certified by peer review) is the author/funder, who has granted bioRxiv a license to display the preprint in perpetuity. It is made available under aCC-BY 4.0 International license.

403 window method does not necessarily indicate non-stationary dynamics of resting brain
404 network (Hindriks et al. 2016). However, in terms of spontaneous neuronal activity
405 itself, there is substantial evidences showing that spontaneous neuronal activity is
406 non-stationary (Foster and Wilson 2006; Ji and Wilson 2007; Logothetis et al. 2012). In
407 particular, under both awake and anesthetized states, transient neuronal events such as
408 sharp-wave-ripples have been shown to produce coordinated activity across the entire
409 brain (Logothetis et al. 2012). The present results are consistent with these previous
410 studies supporting the non-stationarity of neuronal activity, and further showed that FC
411 calculated using such non-stationary neuronal activity also showed non-stationarity, as
412 expected.
413
414 ***Limitations of the study***
415 It should be clearly stated that the present results do not guarantee that sliding window
416 methods are always capable of detecting non-stationarity in human resting-state fMRI
417 data. The present study used tightly head-restrained animals and high signal to
418 noise-ration (SNR) imaging at a high frame rate (5 and 10 Hz for hemodynamics and
419 calcium signal, respectively). Compared to the present experimental conditions, overall
420 SNR in typical human resting-state fMRI is likely to be substantially compromised.
421 Under such low SNR conditions, it is not clear whether simple sliding window
422 correlation methods can detect the non-stationarity of FC (Hindriks et al. 2016;
423 Laumann et al. 2016). With respect to SNR, we expect that the recent development of
424 high-speed fMRI (Feinberg et al. 2010) will significantly improve the detectability of
425 non-stationarity. Nevertheless, the present results suggest that, rather than the sliding
426 window based method, an alternative analysis strategy that directly extracts CAPs from
427 hemodynamic signals (Karahanoğlu and Van De Ville 2015; Liu et al. 2013; Liu and
428 Duyn 2013; Tagliazucchi et al. 2012a) may be more appropriate for extracting relevant
429 information related to the dynamics of FC.
430 It should also be noted that the present results do not claim that dynamic FC has
431 significant behavioral or cognitive consequences. Instead of examining the potential
432 relationship between dynamic FC and cognitive dynamics or behavioral variability [see
433 for recent review (Preti et al. 2016)], here we focused on validating the neuronal origin
434 of dynamic FC. Experiments under anesthesia greatly reduced potential confounding
435 factors, such as head motion and arousal state (Hutchison et al. 2014; Laumann et al.

bioRxiv preprint doi: https://doi.org/10.1101/169698; this version posted July 28, 2017. The copyright holder for this preprint (which was not certified by peer review) is the author/funder, who has granted bioRxiv a license to display the preprint in perpetuity. It is made available under aCC-BY 4.0 International license.

436 2016). Nevertheless, the present wide-field imaging setup can be naturally extended to
437 awake imaging with task-performing mice (Ferezou et al. 2007; Wekselblatt et al. 2016).
438 Such experiments would reveal the potential consequences of the dynamics of FC on its
439 behavioral outcome.
440

bioRxiv preprint doi: https://doi.org/10.1101/169698; this version posted July 28, 2017. The copyright holder for this preprint (which was not certified by peer review) is the author/funder, who has granted bioRxiv a license to display the preprint in perpetuity. It is made available under aCC-BY 4.0 International license.

Acknowledgements

We thank A. Honda and Y. Sono for animal care and genotyping; the Research Support Center, Graduate School of Medical Sciences, Kyushu University, for technical support: and K. Jimura and Y. Noro for helpful discussion. Support for this work was provided by grants from Brain Mapping by Integrated Neurotechnologies for Disease Studies (Brain/MINDS) – Japan Agency for Medical Research and Development (AMED), Core Research for Evolutionary Science and Technology (CREST) – AMED and Strategic International Research Cooperative Program (SCIP) – AMED, and Japan Society for Promotions of Sciences (JSPS) KAKENHI Grants 25221001 and 25117004 (to K.O.); JSPS KAKENHI Grant 17K14931 (to T. Matsui) and JSPS Research Fellowship 20153597 (to T. Murakami).

bioRxiv preprint doi: https://doi.org/10.1101/169698; this version posted July 28, 2017. The copyright holder for this preprint (which was not certified by peer review) is the author/funder, who has granted bioRxiv a license to display the preprint in perpetuity. It is made available under aCC-BY 4.0 International license.

References

Adachi Y, Osada T, Sporns O, Watanabe T, Matsui T, Miyamoto K, Miyashita Y. 2012. Functional connectivity between anatomically unconnected areas is shaped by collective network-level effects in the macaque cortex. Cereb Cortex. 22(7):1586-1592.

Allen EA, Damaraju E, Plis SM, Erhardt EB, Eichele T, Calhoun VD. 2014. Tracking whole-brain connectivity dynamics in the resting state. Cereb Cortex. 24(3):663-676.

Bianciardi M, Fukunaga M, van Gelderen P, Horovitz SG, de Zwart JA, Shmueli K, Duyn JH. 2009. Sources of functional magnetic resonance imaging signal fluctuations in the human brain at rest: A 7 t study. Magn Reson Imaging. 27(8):1019-1029.

Biswal B, Yetkin FZ, Haughton VM, Hyde JS. 1995. Functional connectivity in the motor cortex of resting human brain using echo-planar mri. Magn Reson Med. 34(4):537-541.

Calhoun VD, Miller R, Pearlson G, Adalı T. 2014. The chronnectome: Time-varying connectivity networks as the next frontier in fmri data discovery. Neuron. 84(2):262-274.

Chang C, Cunningham JP, Glover GH. 2009. Influence of heart rate on the bold signal: The cardiac response function. Neuroimage. 44(3):857-869.

Chang C, Glover GH. 2009. Relationship between respiration, end-tidal co2, and bold signals in resting-state fmri. Neuroimage. 47(4):1381-1393.

Chang C, Glover GH. 2010. Time-frequency dynamics of resting-state brain connectivity measured with fmri. Neuroimage. 50(1):81-98.

Chang C, Liu Z, Chen MC, Liu X, Duyn JH. 2013. Eeg correlates of time-varying bold functional connectivity. Neuroimage. 72:227-236.

Deco G, Ponce-Alvarez A, Mantini D, Romani GL, Hagmann P, Corbetta M. 2013. Resting-state functional connectivity emerges from structurally and dynamically shaped slow linear fluctuations. J Neurosci. 33(27):11239-11252.

Feinberg DA, Moeller S, Smith SM, Auerbach E, Ramanna S, Gunther M, Glasser MF, Miller KL, Ugurbil K, Yacoub E. 2010. Multiplexed echo

bioRxiv preprint doi: https://doi.org/10.1101/169698; this version posted July 28, 2017. The copyright holder for this preprint (which was not certified by peer review) is the author/funder, who has granted bioRxiv a license to display the preprint in perpetuity. It is made available under aCC-BY 4.0 International license.

planar imaging for sub-second whole brain fmri and fast diffusion imaging. PLoS One. 5(12):e15710.

Ferezou I, Haiss F, Gentet LJ, Aronoff R, Weber B, Petersen CC. 2007. Spatiotemporal dynamics of cortical sensorimotor integration in behaving mice. Neuron. 56(5):907-923.

Foster DJ, Wilson MA. 2006. Reverse replay of behavioural sequences in hippocampal place cells during the awake state. Nature. 440(7084):680-683.

Fox MD, Raichle ME. 2007. Spontaneous fluctuations in brain activity observed with functional magnetic resonance imaging. Nat Rev Neurosci. 8(9):700-711.

Fox MD, Snyder AZ, Vincent JL, Corbetta M, Van Essen DC, Raichle ME. 2005. The human brain is intrinsically organized into dynamic, anticorrelated functional networks. Proc Natl Acad Sci U S A. 102(27):9673-9678.

Glover GH, Li TQ, Ress D. 2000. Image-based method for retrospective correction of physiological motion effects in fmri: Retroicor. Magn Reson Med. 44(1):162-167.

Hansen EC, Battaglia D, Spiegler A, Deco G, Jirsa VK. 2015. Functional connectivity dynamics: Modeling the switching behavior of the resting state. Neuroimage. 105:525-535.

Hindriks R, Adhikari MH, Murayama Y, Ganzetti M, Mantini D, Logothetis NK, Deco G. 2016. Can sliding-window correlations reveal dynamic functional connectivity in resting-state fmri? Neuroimage. 127:242-256.

Honey CJ, Sporns O, Cammoun L, Gigandet X, Thiran JP, Meuli R, Hagmann P. 2009. Predicting human resting-state functional connectivity from structural connectivity. Proc Natl Acad Sci U S A. 106(6):2035-2040.

Hutchison RM, Hutchison M, Manning KY, Menon RS, Everling S. 2014. Isoflurane induces dose-dependent alterations in the cortical connectivity profiles and dynamic properties of the brain's functional architecture. Hum Brain Mapp. 35(12):5754-5775.

bioRxiv preprint doi: https://doi.org/10.1101/169698; this version posted July 28, 2017. The copyright holder for this preprint (which was not certified by peer review) is the author/funder, who has granted bioRxiv a license to display the preprint in perpetuity. It is made available under aCC-BY 4.0 International license.

518 Hutchison RM, Womelsdorf T, Allen EA, Bandettini PA, Calhoun VD,
519 Corbetta M, Della Penna S, Duyn JH, Glover GH, Gonzalez-Castillo J
520 et al. 2013. Dynamic functional connectivity: Promise, issues, and
521 interpretations. Neuroimage. 80:360-378.
522 Ji D, Wilson MA. 2007. Coordinated memory replay in the visual cortex and
523 hippocampus during sleep. Nat Neurosci. 10(1):100-107.
524 Karahanoğlu FI, Van De Ville D. 2015. Transient brain activity disentangles
525 fmri resting-state dynamics in terms of spatially and temporally
526 overlapping networks. Nat Commun. 6:7751.
527 Laumann TO, Snyder AZ, Mitra A, Gordon EM, Gratton C, Adeyemo B,
528 Gilmore AW, Nelson SM, Berg JJ, Greene DJ et al. 2016. On the
529 stability of bold fmri correlations. Cereb Cortex.
530 Liu X, Chang C, Duyn JH. 2013. Decomposition of spontaneous brain
531 activity into distinct fmri co-activation patterns. Front Syst Neurosci.
532 7:101.
533 Liu X, Duyn JH. 2013. Time-varying functional network information
534 extracted from brief instances of spontaneous brain activity. Proc Natl
535 Acad Sci U S A. 110(11):4392-4397.
536 Logothetis NK, Eschenko O, Murayama Y, Augath M, Steudel T, Evrard HC,
537 Besserve M, Oeltermann A. 2012. Hippocampal-cortical interaction
538 during periods of subcortical silence. Nature. 491(7425):547-553.
539 Lu H, Zuo Y, Gu H, Waltz JA, Zhan W, Scholl CA, Rea W, Yang Y, Stein EA.
540 2007. Synchronized delta oscillations correlate with the resting-state
541 functional mri signal. Proc Natl Acad Sci U S A. 104(46):18265-18269.
542 Majeed W, Magnuson M, Keilholz SD. 2009. Spatiotemporal dynamics of low
543 frequency fluctuations in bold fmri of the rat. J Magn Reson Imaging.
544 30(2):384-393.
545 Matsui T, Koyano KW, Tamura K, Osada T, Adachi Y, Miyamoto K, Chikazoe
546 J, Kamigaki T, Miyashita Y. 2012. Fmri activity in the macaque
547 cerebellum evoked by intracortical microstimulation of the primary
548 somatosensory cortex: Evidence for polysynaptic propagation. PLoS
549 One. 7(10):e47515.
550 Matsui T, Murakami T, Ohki K. 2016. Transient neuronal coactivations

bioRxiv preprint doi: https://doi.org/10.1101/169698; this version posted July 28, 2017. The copyright holder for this preprint (which was not certified by peer review) is the author/funder, who has granted bioRxiv a license to display the preprint in perpetuity. It is made available under aCC-BY 4.0 International license.

551 embedded in globally propagating waves underlie resting-state
552 functional connectivity. Proc Natl Acad Sci U S A. 113(23):6556-6561.
553 Matsui T, Tamura K, Koyano KW, Takeuchi D, Adachi Y, Osada T, Miyashita
554 Y. 2011. Direct comparison of spontaneous functional connectivity and
555 effective connectivity measured by intracortical microstimulation: An
556 fmri study in macaque monkeys. Cereb Cortex. 21(10):2348-2356.
557 Messé A, Rudrauf D, Benali H, Marrelec G. 2014. Relating structure and
558 function in the human brain: Relative contributions of anatomy,
559 stationary dynamics, and non-stationarities. PLoS Comput Biol.
560 10(3):e1003530.
561 Mohajerani MH, Chan AW, Mohsenvand M, LeDue J, Liu R, McVea DA,
562 Boyd JD, Wang YT, Reimers M, Murphy TH. 2013. Spontaneous
563 cortical activity alternates between motifs defined by regional axonal
564 projections. Nat Neurosci. 16(10):1426-1435.
565 Murakami T, Yoshida T, Matsui T, Ohki K. 2015. Wide-field ca(2+) imaging
566 reveals visually evoked activity in the retrosplenial area. Front Mol
567 Neurosci. 8:20.
568 Pan WJ, Thompson G, Magnuson M, Majeed W, Jaeger D, Keilholz S. 2011.
569 Broadband local field potentials correlate with spontaneous
570 fluctuations in functional magnetic resonance imaging signals in the
571 rat somatosensory cortex under isoflurane anesthesia. Brain Connect.
572 1(2):119-131.
573 Preti MG, Bolton TA, Van De Ville D. 2016. The dynamic functional
574 connectome: State-of-the-art and perspectives. Neuroimage.
575 Shmueli K, van Gelderen P, de Zwart JA, Horovitz SG, Fukunaga M, Jansma
576 JM, Duyn JH. 2007. Low-frequency fluctuations in the cardiac rate as
577 a source of variance in the resting-state fmri bold signal. Neuroimage.
578 38(2):306-320.
579 Tagliazucchi E, Balenzuela P, Fraiman D, Chialvo DR. 2012a. Criticality in
580 large-scale brain fmri dynamics unveiled by a novel point process
581 analysis. Front Physiol. 3:15.
582 Tagliazucchi E, Balenzuela P, Fraiman D, Montoya P, Chialvo DR. 2011.
583 Spontaneous bold event triggered averages for estimating functional

bioRxiv preprint doi: https://doi.org/10.1101/169698; this version posted July 28, 2017. The copyright holder for this preprint (which was not certified by peer review) is the author/funder, who has granted bioRxiv a license to display the preprint in perpetuity. It is made available under aCC-BY 4.0 International license.

584 connectivity at resting state. Neurosci Lett. 488(2):158-163.
585 Tagliazucchi E, von Wegner F, Morzelewski A, Brodbeck V, Laufs H. 2012b.
586 Dynamic bold functional connectivity in humans and its
587 electrophysiological correlates. Front Hum Neurosci. 6:339.
588 Thompson GJ, Merritt MD, Pan WJ, Magnuson ME, Grooms JK, Jaeger D,
589 Keilholz SD. 2013. Neural correlates of time-varying functional
590 connectivity in the rat. Neuroimage. 83:826-836.
591 Tohmi M, Meguro R, Tsukano H, Hishida R, Shibuki K. 2014. The
592 extrageniculate visual pathway generates distinct response properties
593 in the higher visual areas of mice. Curr Biol. 24(6):587-597.
594 Van Dijk KR, Hedden T, Venkataraman A, Evans KC, Lazar SW, Buckner RL.
595 2010. Intrinsic functional connectivity as a tool for human
596 connectomics: Theory, properties, and optimization. J Neurophysiol.
597 103(1):297-321.
598 Vanni MP, Murphy TH. 2014. Mesoscale transcranial spontaneous activity
599 mapping in gcamp3 transgenic mice reveals extensive reciprocal
600 connections between areas of somatomotor cortex. J Neurosci.
601 34(48):15931-15946.
602 Vincent JL, Patel GH, Fox MD, Snyder AZ, Baker JT, Van Essen DC, Zempel
603 JM, Snyder LH, Corbetta M, Raichle ME. 2007. Intrinsic functional
604 architecture in the anaesthetized monkey brain. Nature.
605 447(7140):83-86.
606 Wekselblatt JB, Flister ED, Piscopo DM, Niell CM. 2016. Large-scale
607 imaging of cortical dynamics during sensory perception and behavior.
608 J Neurophysiol. 115(6):2852-2866.
609 White BR, Bauer AQ, Snyder AZ, Schlaggar BL, Lee JM, Culver JP. 2011.
610 Imaging of functional connectivity in the mouse brain. PLoS One.
611 6(1):e16322.
612 Zalesky A, Fornito A, Cocchi L, Gollo LL, Breakspear M. 2014. Time-resolved
613 resting-state brain networks. Proc Natl Acad Sci U S A.
614 111(28):10341-10346.
615 Zariwala HA, Borghuis BG, Hoogland TM, Madisen L, Tian L, De Zeeuw CI,
616 Zeng H, Looger LL, Svoboda K, Chen TW. 2012. A cre-dependent

bioRxiv preprint doi: https://doi.org/10.1101/169698; this version posted July 28, 2017. The copyright holder for this preprint (which was not certified by peer review) is the author/funder, who has granted bioRxiv a license to display the preprint in perpetuity. It is made available under aCC-BY 4.0 International license.

617 gcamp3 reporter mouse for neuronal imaging in vivo. J Neurosci.
618 32(9):3131-3141.
619
620

bioRxiv preprint doi: https://doi.org/10.1101/169698; this version posted July 28, 2017. The copyright holder for this preprint (which was not certified by peer review) is the author/funder, who has granted bioRxiv a license to display the preprint in perpetuity. It is made available under aCC-BY 4.0 International license.

Figure Captions

Figure 1. Representative dynamics of simultaneously observed calcium and hemodynamic FC. (A) Experimental setup. The left most panel shows the setup for simultaneous imaging. Right side shows example calcium time courses for two ROIs (green and cyan traces indicate M1 and V1 ROIs, respectively. Positions of the ROIs indicated in the example field of view. See Supplementary Figure 1 for abbreviations). FC with short time window uses subset of frames contained in short (30 sec) windows (red dotted squares). Sliding FC for hemodynamic signal was carried out similarly. **(B)-(C)** Examples dynamics of calcium and hemodynamic FC. (B) FC between right V1 and right AC. (C) FC between left M1 and left pPar. See Supplementary Figure 1 for ROI positions and abbreviations. **(D)** Histogram of correlation between time courses of Ca-FC and Hemo-FC for the data (solid line) and the scan-shifted control (dotted line). Data from all pairs of ROIs for all scans obtained in all mice were used.

Figure 2. Significant relationship between calcium and hemodynamic FC calculated in short time windows. (A)-(B) Example ROI-by-ROI FC matrices for calcium and hemodynamics for different (non-overlapping) 30 sec windows. FC matrices were similar for calcium and hemodynamics in the same time window, but not across different time windows. **(C)** Cumulative histogram of correlation between FC matrices for calcium and hemodynamics. Dotted line indicates trial-shifted control. **(D)** Correlation between FC matrices for calcium and hemodynamics was larger for the data than for the trial-shifted control significantly across animals. **(E)** Correlation between FC matrices of calcium and hemodynamics was larger for the data than the trial-shifted control across different window-sizes (1, 2, 3, 5, 6, 10, 12, 15, 20, 30 and 60 sec). Error bars indicate s.e.m. across animals (n = 7).

Figure 3. Comparison of calcium CAPs and hemodynamic FC across time-windows. (A) Procedure for detection of CAPs in calcium signal. For a given ROI, a calcium time course was extracted and z normalized (green time courses). Then, peaks exceeding 2 s.d. (red dots) were extracted. The frames corresponding to the peaks were considered CAPs (panels above the time courses). For each window, CAPs in calcium signal were averaged to obtain mean calcium CAP. Hemodynamic CAPs were calculated similarly (see Methods). Maps of Ca-FC and Hemo-FC were also calculated

bioRxiv preprint doi: https://doi.org/10.1101/169698; this version posted July 28, 2017. The copyright holder for this preprint (which was not certified by peer review) is the author/funder, who has granted bioRxiv a license to display the preprint in perpetuity. It is made available under aCC-BY 4.0 International license.

using the same time window. **(B)** Schematics to show the procedure of comparing calcium CAP and Hemo-FC across all ROI pairs in each time window. In each 30 sec time window, mean calcium CAPs and Hemo-FC maps were calculated for all ROIs as seeds (left). Then, for each seed-ROI j, calcium CAP and Hemo-FC values in ROI i were extracted to obtain a pair of CAP-FC values for the ROI-pairs (i, j) (middle). Finally, for each time-window, CAP-FC values were compared across all pairs of ROIs (right). **(C)** Histograms of correlation between CAP and Hemo-FC for all time windows across all animals. Vertical line indicates mean across time windows. **(D)** Mean correlation between CAP and Hemo-FC across animals. Error bar indicates s.e.m. across animals (n = 7).

Figure 4. Temporal fluctuations in calcium CAPs and Hemo-FC was significantly related. (A) Schematics of the analysis. In each 30 sec time-window, mean calcium CAP and Hemo-FC were calculated (indicated as window CAP and window FC, respectively). From window CAP and window FC, average calcium CAP and average Hemo-FC that were calculated using the entire scan, in which the 30-sec window belongs to, were subtracted to obtain maps of ΔCAP and ΔFC, respectively. Finally, values of ΔCAP and ΔFC were compared across ROI pairs similarly as in Figure 3B. **(B)** Histograms of correlation between ΔCAP and ΔFC for all time windows across all animals. Vertical lines indicate mean across time windows. Solid and dotted lines indicate real and trial-shifted data, respectively. **(C)** Correlation between ΔCAP and ΔFC was significantly larger for the data than for trial-shifted control across animals. **(D)** Same as (C) but with different window-sizes (1, 2, 3, 5, 6, 10, 12, 15, 20, 30 and 60 sec). Error bars indicate s.e.m. across animals (n = 7).

Figure 5. Comparison with simulated data indicated non-stationarity of the real data. (A) Examples of real and simulated time courses. Simulated time course (black) was matched to real data (green; calcium) in mean spectral content (middle panels) and ROI-by-ROI covariance matrix (right panels). The same procedure was applied to create simulated hemodynamic data (not shown). **(B)** Cluster validity index calculated for different number of clusters (k = 2-10). In both calcium (left) and hemodynamics (right), the cluster validity index was smaller for the real (solid lines) than the simulated data (dotted lines) indicating that the real data tended to be more clustered. **(C)** Kurtosis

bioRxiv preprint doi: https://doi.org/10.1101/169698; this version posted July 28, 2017. The copyright holder for this preprint (which was not certified by peer review) is the author/funder, who has granted bioRxiv a license to display the preprint in perpetuity. It is made available under aCC-BY 4.0 International license.

of real and simulated covariance matrices. For both calcium (left) and hemodynamics (right), multivariate kurtosis was larger for the real than for the simulated data. Error bars indicate s.e.m. across animals (n = 7).

Supplementary Figure 1. Anatomical locations of ROIs. Anatomical locations of 19 ROIs are shown for the right hemisphere. Anatomical nomenclatures of ROIs are shown on the right. ROIs in the left hemisphere are taken at mirror symmetric positions to yield a total of 38 ROIs.

bioRxiv preprint doi: https://doi.org/10.1101/169698; this version posted July 28, 2017. The copyright holder for this preprint (which was not certified by peer review) is the author/funder, who has granted bioRxiv a license to display the preprint in perpetuity. It is made available under aCC-BY 4.0 International license.

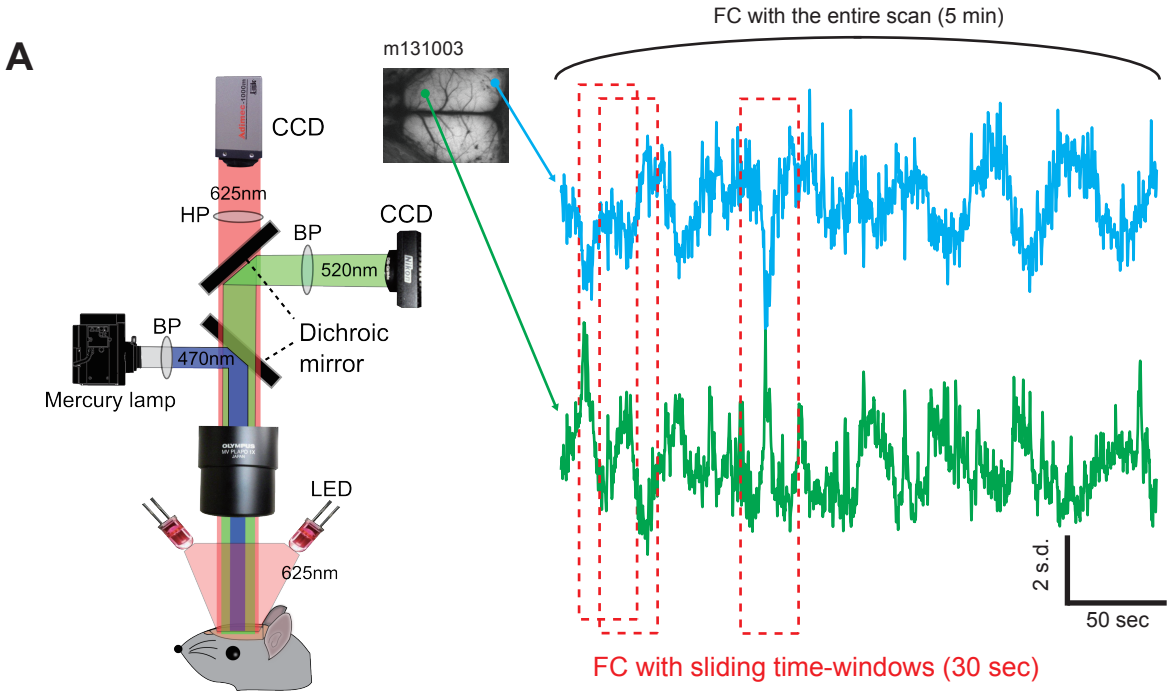

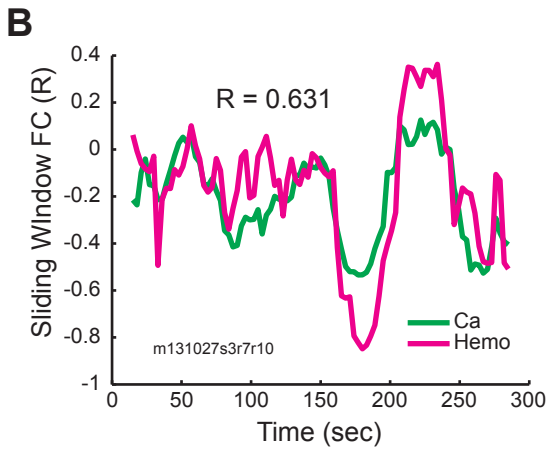

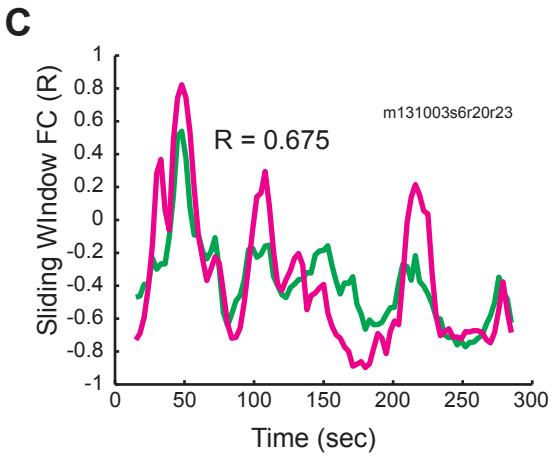

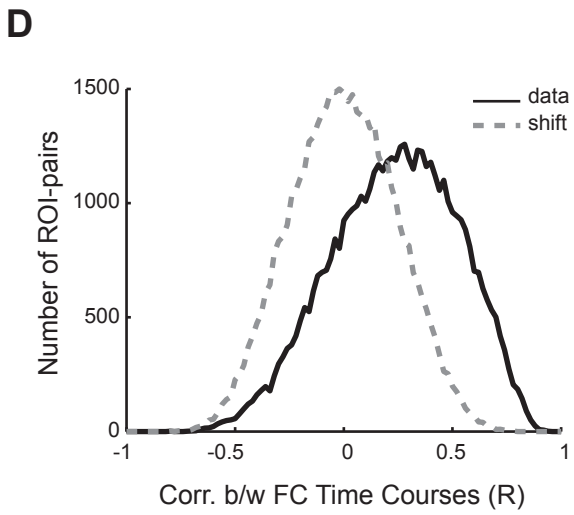

Figure 1

bioRxiv preprint doi: https://doi.org/10.1101/169698; this version posted July 28, 2017. The copyright holder for this preprint (which was not certified by peer review) is the author/funder, who has granted bioRxiv a license to display the preprint in perpetuity. It is made available under aCC-BY 4.0 International license.

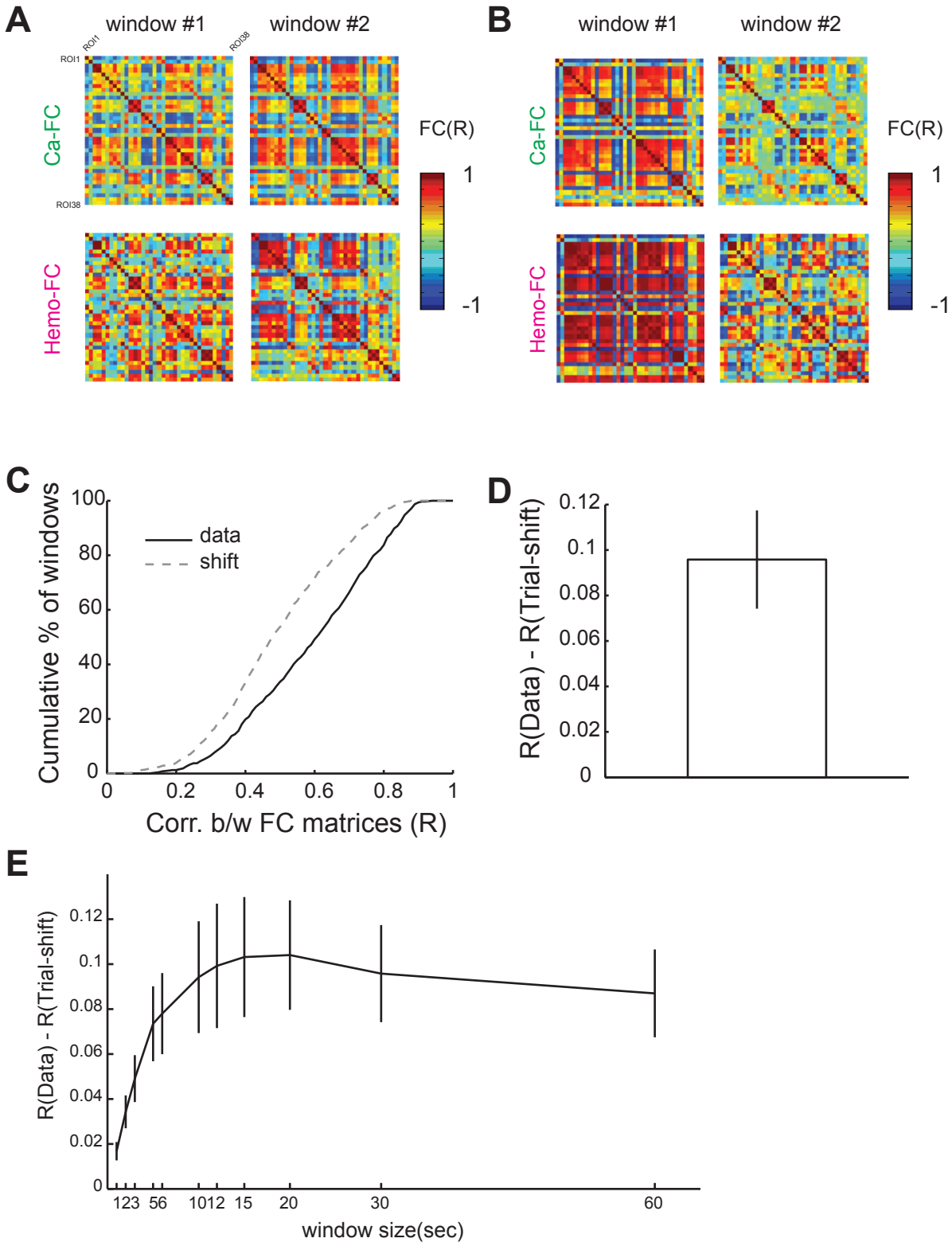

Figure 2

bioRxiv preprint doi: https://doi.org/10.1101/169698; this version posted July 28, 2017. The copyright holder for this preprint (which was not certified by peer review) is the author/funder, who has granted bioRxiv a license to display the preprint in perpetuity. It is made available under aCC-BY 4.0 International license.

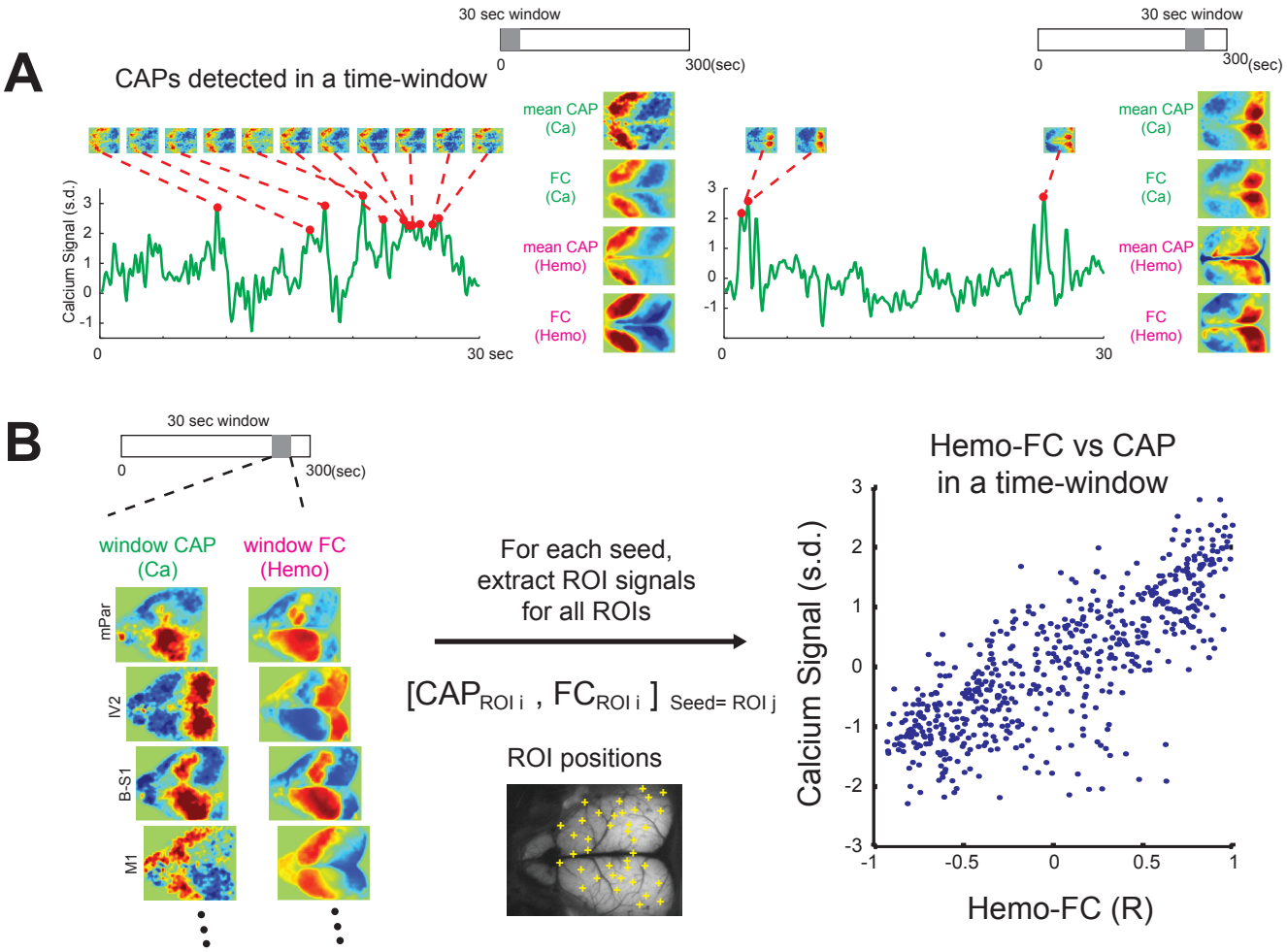

Figure 3

bioRxiv preprint doi: https://doi.org/10.1101/169698; this version posted July 28, 2017. The copyright holder for this preprint (which was not certified by peer review) is the author/funder, who has granted bioRxiv a license to display the preprint in perpetuity. It is made available under aCC-BY 4.0 International license.

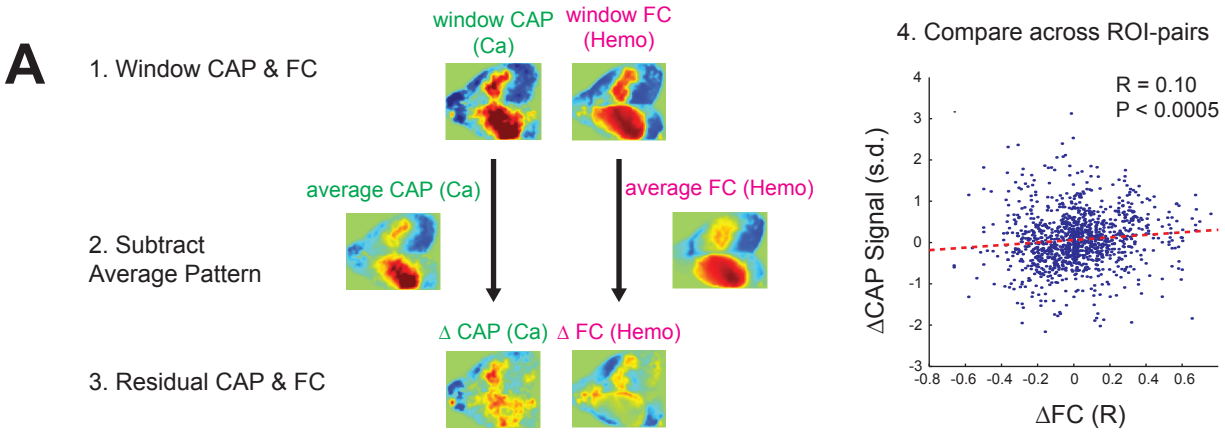

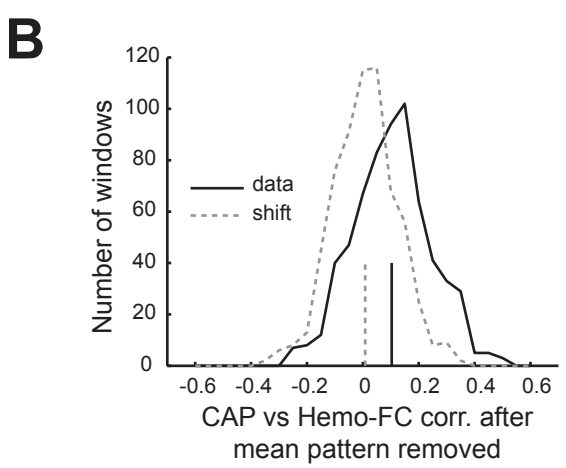

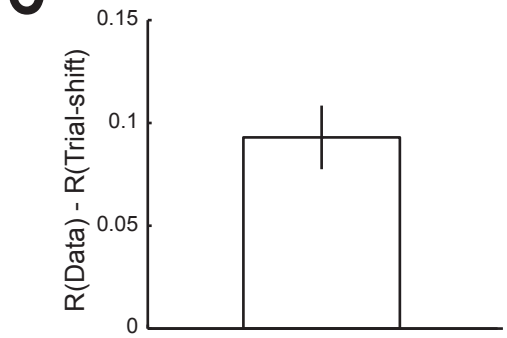

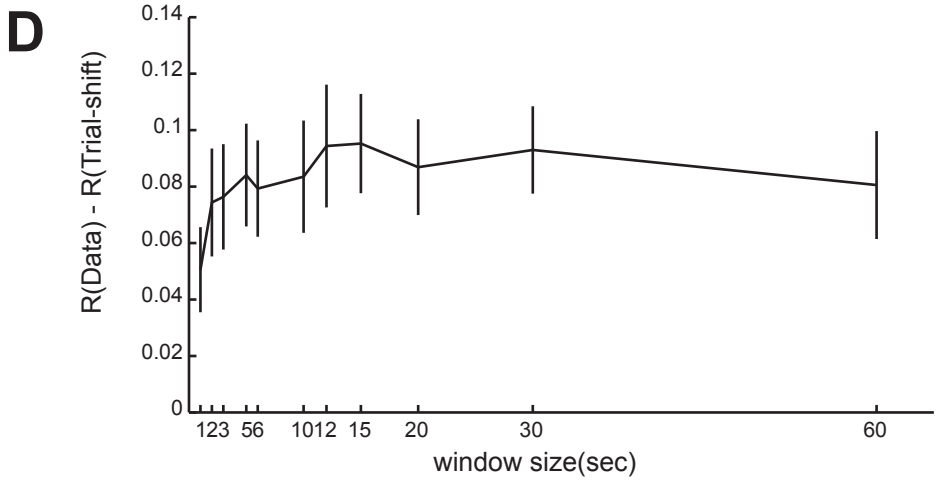

Figure 4

bioRxiv preprint doi: https://doi.org/10.1101/169698; this version posted July 28, 2017. The copyright holder for this preprint (which was not certified by peer review) is the author/funder, who has granted bioRxiv a license to display the preprint in perpetuity. It is made available under aCC-BY 4.0 International license.

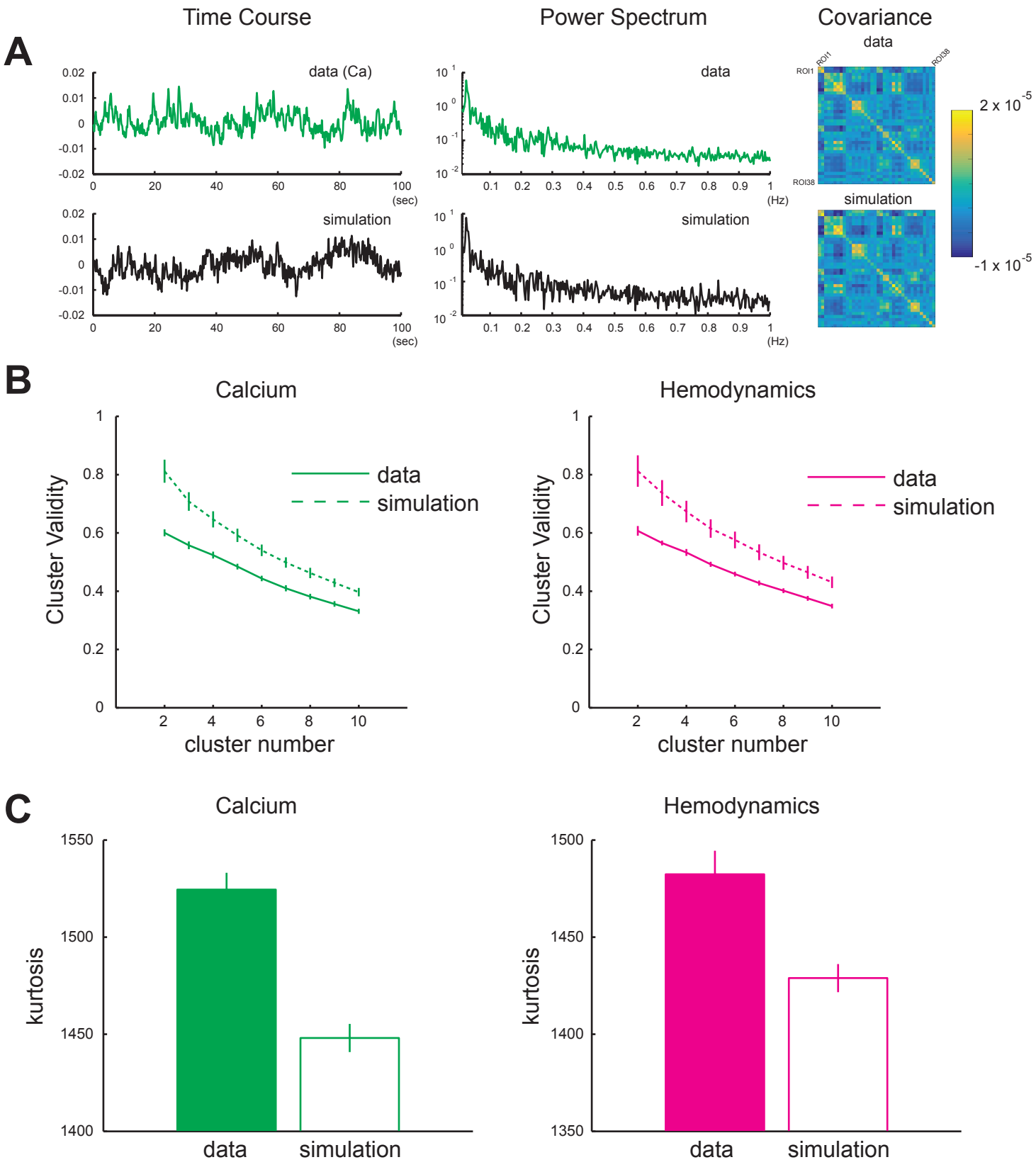

Figure 5

bioRxiv preprint doi: https://doi.org/10.1101/169698; this version posted July 28, 2017. The copyright holder for this preprint (which was not certified by peer review) is the author/funder, who has granted bioRxiv a license to display the preprint in perpetuity. It is made available under aCC-BY 4.0 International license.

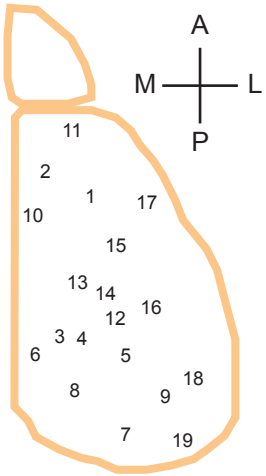

1. Primary Motor Area (M1)
2. Secondary Motor Area (M2)
3. Parietal Medial Area (mPar)
4. Parietal Lateral Area (lPar)
5. Parietal Posterior Area (pPar)
6. Restrosplenial Area (Rsp)
7. Primary Visual Area (V1)
8. Medial Secondary Visual Area (mV2)
9. Lateral Secondary VIsual Area (lV2)
10. Anterior Cingulate Area (AC)
11. Frontal Association Area (FAsc)
12. Trunk Region of Primary Somatosensory Area (Tr-S1)
13. Hindlimb Region of Primary Somatosensory Area (HL-S1)
14. Shoulder Region of Primary Somatosensory Area (Sh-S1)
15. Forelimb Region of Primary Somatosensory Area (FL-S1)
16. Barrel Region of Primary Somatosensory Area (B-S1)
17. Head Region of Primary Somatosensory Area (H-S1)
18. Auditory Area (Aud)
19. Temporal Association Area (TA)

Supplementary Figure 1